JOURNAL OF GEOPHYSICAL RESEARCH, VOL. 114, C02017, doi:10.1029/2007JC004642, 2009

Shelfbreak frontal eddies over the continental slope north of Cape Hatteras

James H. Churchill[1] and Glen Gawarkiewicz[1]

Received 14 November 2007; revised 1 August 2008; accepted 20 August 2008; published 20 February 2009.

[1] Shelfbreak and slope eddies have been implicated as important agents in the exchange of water between the shelf and slope domains of the Middle Atlantic Bight (MAB). Here we present temperature, salinity, and velocity data from a series of shipboard transects that intercepted a rich eddy field over the slope of the southern MAB. Attention is focused on a well-sampled cyclonic eddy, of roughly 60-km diameter and 300-m depth, that translated southward at 0.1 m s^{-1}. The eddy was composed of a mix of water masses including MAB shelf and slope water, Gulf Stream water, and water from the MAB shelfbreak front. Gradient Richardson numbers suggest that these water masses were subject to vigorous turbulent vertical mixing. The transport of shelfbreak frontal water contained within the eddy was substantial. In the upper 100 m, shelfbreak frontal water comprised ~75% of the eddy's volume. This frontal water fraction moved southward with a transport of ~0.4 Sv, comparable with the volume transport within the shelfbreak frontal jet. A number of factors indicate that this highly energetic eddy, with maximum azimuthal velocity of 0.7 m s^{-1}, was generated through instability of the shelfbreak frontal jet. The eddy had apparently developed rapidly (in <3 days), consistent with models of eddy generation through baroclinic instability of the shelfbreak frontal jet. The eddy's potential temperature/salinity (θ/S) properties and energy density closely matched the θ/S properties and energy density found in the frontal jet to the north of the eddy.

Citation: Churchill, J. H., and G. Gawarkiewicz (2009), Shelfbreak frontal eddies over the continental slope north of Cape Hatteras, *J. Geophys. Res.*, *114*, C02017, doi:10.1029/2007JC004642.

1. Introduction

[2] It has long been recognized that the shelf waters off eastern Canada and the northeastern United States are separated from the warmer and more saline waters offshore by a surface to bottom front that intersects the seafloor near the shelfbreak [*Libby*, 1891; *Bigelow*, 1933]. Associated with the front is a strong equatorward current, the shelfbreak frontal jet. Studies conducted in the Middle Atlantic Bight (MAB), which stretches from Georges Bank to Cape Hatteras, indicate that the frontal jet transports water at a mean rate of roughly 0.25 Sv and has mean near-surface velocities of order 0.3 m s^{-1} [*Linder and Gawarkiewicz*, 1998; *Fratantoni et al.*, 2001].

[3] Although the shelf edge front is a permanent feature, it is not an impermeable barrier. Shelf/slope water exchange is revealed by along-shelf changes in the properties of shelf water, which is transported southward toward Cape Hatteras. Loss of MAB shelf water to the slope region is revealed by a southward reduction in the shelf water volume transport, from ~0.4 Sv off southern New England to ~0.2 Sv off Maryland [*Beardsley and Boicourt*, 1981; *Biscaye et al.*, 1994]. Conversely, an influx of slope water into the shelf water mass is indicated by an increase in mean salinity and oxygen isotope ratio in shelf water going from Cape Cod to Cape Hatteras [*Fairbanks*, 1982; *Chapman*, 1986].

[4] Eddies formed near the shelfbreak have been implicated as an important means of exchange across the shelfbreak front. The effect of shelfbreak eddies on the delivery of slope water to the shelf was examined by *Churchill et al.* [2003]. Their study focused on slope water intrusions onto the southern flank of Georges Bank that were associated with small-scale eddies and/or sharply crested meanders of the shelfbreak front, extending onto the flank.

[5] The impact of eddies on shelf water export to the slope region has been explored by *Houghton et al.* [1986] and *Garvine et al.* [1988]. Both groups of investigators examined eddies that appeared over the shelf edge and upper slope south of New England and carried shelf water seaward of the shelfbreak front. The study of Houghton et al. was confined to a small, highly energetic (peak azimuthal velocity of 0.5 m s^{-1}) anticyclonic eddy; whereas Garvine et al. examined a series of cyclonic and somewhat weaker eddies. Garvine et al. and Houghton et al. postulated that the apparently detached parcels of MAB shelf water, often seen in hydrographic observations over the MAB slope, may actually be water drawn seaward by the circulation of shelfbreak eddies. In a more recent study, *Flagg et al.* [1998] offered further evidence of MAB shelf water export associated with a shelfbreak eddy. They examined an anticyclonic eddy that appeared over the slope of the southern MAB and contained a large quantity of subthermocline (cold pool) water from the MAB shelf.

[1]Department of Physical Oceanography, Woods Hole Oceanographic Institution, Woods Hole, Massachusetts, USA.

0148-0227/09/2007JC004642$09.00

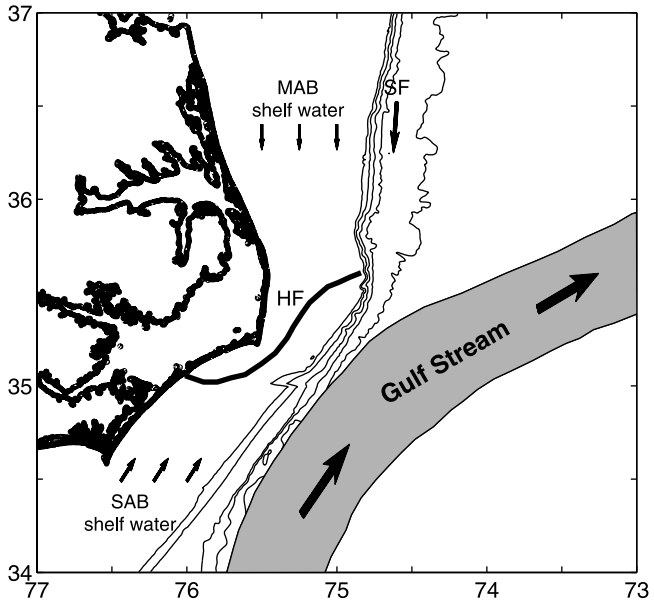

Figure 1. Diagram of the Cape Hatteras shelf/slope region with a simplified representation of the area's principal currents. The arrows over the shelf show the long-term mean flows of Middle Atlantic Bight (MAB) and South Atlantic Bight (SAB) shelf water, whereas the arrow over the MAB slope shows the flow of the shelfbreak frontal (SF) jet. The line labeled HF represents the Hatteras Front.

[6] A number of investigators have commented on possible mechanisms by which shelfbreak eddies may be generated. *Houghton et al.* [1986] postulated that the anticyclonic vorticity of the eddy they observed was produced through thinning of a parcel of shelf water as it moved seaward. The eddies observed by *Garvine et al.* [1988] appeared to develop from meanders of the shelfbreak front. *Churchill et al.* [2003] posited that instability of the shelfbreak frontal jet, due to interaction with a Gulf Stream warm-core ring, was responsible for the eddies they observed off of Georges Bank.

[7] Here we examine a rich eddy field that appeared over the slope of the southern MAB during January 2005 and was intercepted by a series of acoustic Doppler current profiler (ADCP)/conductivity-temperature-depth profiler (CTD) transects. As will be demonstrated, these observations reveal what may be an important mechanism for the export of frontal water to the slope north of Cape Hatteras. Focusing on a particularly well-sampled eddy, we examine the eddy's azimuthal velocity structure and its departure from a geostrophic balance. Also analyzed are the water mass distribution and the propensity for turbulent mixing within the eddy. Perhaps most importantly, we utilize the ADCP/CTD survey data to assess the possibility that the eddy, and the larger eddy field in which it was embedded, were generated through instability of the shelfbreak jet.

2. Oceanographic Setting

[8] Our study was conducted in a highly complex oceanographic region, which encompasses a number of distinct currents and water masses (Figure 1). With a northeastward transport of order 90 Sv and maximum velocity of >1.5 m s^{-1} [*Halkin and Rossby*, 1985], the Gulf Stream is the dominant current of the region. After it separates from the continental margin near Cape Hatteras, the Gulf Stream flows over deep water and is often contorted by meanders of varying amplitudes [*Halliwell and Mooers*, 1983; *Pickart and Watts*, 1993]. Other currents of the region are defined by their long-term mean velocities, although it should be noted that these currents may reverse due to wind-forcing. Mean flows approaching Cape Hatteras from the north include the shelfbreak frontal jet, described in section 1, and the southward drift of MAB shelf water. The latter has a transport of order 0.24 Sv in the southern MAB [*Kim et al.*, 2001]. Approaching Cape Hatteras from the south is the mean northward flow of South Atlantic Bight (SAB) shelf water. Separating the MAB and SAB shelf water masses is feature known as the Hatteras Front [*Churchill and Berger*, 1998], which encompasses large horizontal temperature and salinity gradients and extends across the shelf near Cape Hatteras.

[9] A large export of MAB shelf water going southward toward the Hatteras front has been documented by *Churchill and Berger* [1998] and *Kim et al.* [2001]. Some portion of this export is apparently entrained into the flow of the Gulf Stream, as MAB shelf water has frequently been observed along the northern margin of the Stream [*Ford et al.*, 1952; *Churchill et al.*, 1989; *Lillibridge et al.*, 1990].

3. Measurements

[10] The measurements used in our study were acquired as part of the January–February 2005 field study of the Frontal Interaction Near Cape Hatteras (FINCH) program. This was a multiplatform data collection operation that involved deployment of instrumented moorings over the Hatteras Shelf and acquisition of data from two research vessels. One vessel, the R/V *Slover*, concentrated on the nearshore region close to Cape Hatteras; while the other, the R/V *Oceanus*, operated principally over the shelf and slope further to the north. Our study focuses on temperature, salinity and

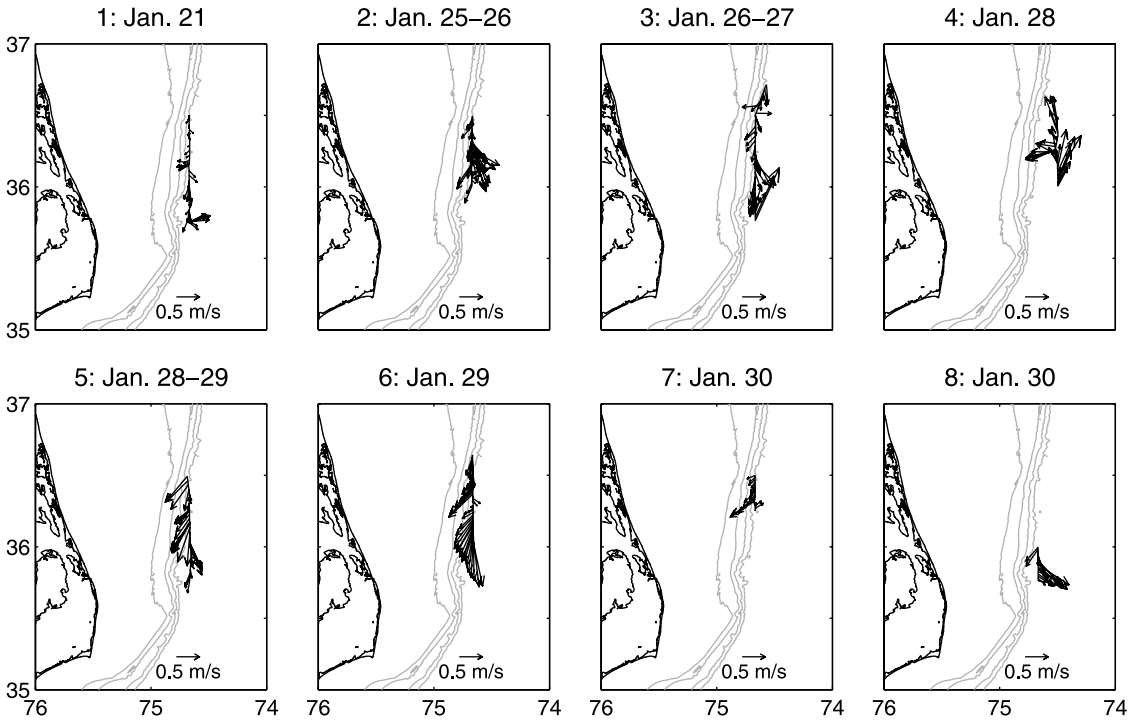

Figure 2. Near-surface velocities measured along the eight north-south slope transects of the FINCH January–February 2005 cruise. The titles give the transect number and date. Velocities are at 17 m along transect 1 and at 19 m along all other transects. Depth contours represent the 50, 100, 500, and 1000-m isobaths and always increase offshore.

water velocity measurements acquired from the R/V *Oceanus* along eight north-south transects extending over the slope region seaward of the 500-m isobath (Figure 2). These are referred to as N–S slope transects 1–8, where the transect number increases in time from the earliest (transect 1) to the latest transect. Seven of the transects are aligned with 74.67°W, and the other is situated further to the east along 74.5°W.

[11] The transect water velocity measurements are from the shipboard ADCP (RD Instruments narrowband 150 KHz ADCP). The ADCP velocities of the first transect (21 January 2005) extend from 17 to 521-m depth and are averages over 8-m depth bins. Because of a change in the setting in the ADCP acquisition software, the velocities acquired over the subsequent seven transects (25–30 January) extend over a depth range of 15–267 m and are averages over 4-m bins. The velocity profiles from all transects are ensemble averages over 5 min intervals.

[12] The temperature and salinity data taken along the slope transects, were acquired either from the shipboard CTD (Sea-Bird Electronics, Inc. model 911+) or from a CTD (also a Sea-Bird model 911+) mounted on a towed undulating vehicle, the Geological and Marine Instrumentation model MKII "Scanfish." The shipboard CTD data were collected with the ship drifting freely and extend over a depth of range of approximately 2–300 m. The Scanfish CTD acquired data with the ship steaming at roughly 6 knots and with the Scanfish undulating roughly between 2 and 120 m depth. Horizontal spacing between the shallowest points of an undulation cycle ranged from 500 m in shallow water to 2 km in deep water. In processing the Scanfish data, measurements from a full undulation (ascending and descending cycles) were averaging into a single vertical profile.

[13] Our analysis also included CTD and ADCP data acquired over a transect that extended over the shelf and slope, along 36.75°N, at the northern extreme of our study area (Figure 3). The data from this transect were used to assess the origin of the water and kinetic energy observed over the N–S slope transects further to the south.

[14] Barotropic tidal currents were removed from all velocities employed in our analysis using results of tidal simulations computed by the finite element model ADCIRC [*Luettich et al.*, 1992] over a North Atlantic model grid [see *Blanton et al.*, 2004]. Over the slope transects, the estimated barotropic tidal currents were always relatively small, <1.2 cm s^{-1}.

4. Evidence of Rapid Eddy Generation Over the Slope

[15] At all vertical levels, the velocity vectors along the N–S slope transects (Figure 2) show an unmistakable temporal pattern marked by a dramatic increase in current strength between the first and second transects (21 to 25 January) and continued strong currents over all subsequent transects (25–30 January). This pattern is quantified by the mean of the squared current speed, proportional to mean kinetic energy, measured over each transect in the 15–267 m depth band (Table 1). The mean squared speed of the first transect is, by far, the smallest of all transects. It is exceeded by roughly a factor of three by the mean squared speed of transect 2 and is bested by a factor of 3.4 by mean squared

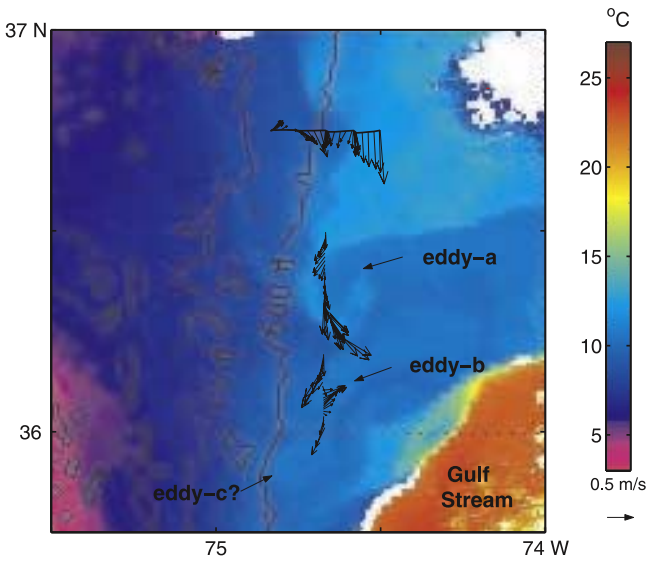

Figure 3. Satellite radiometer-derived SST field of 0245 on 26 January 2005 showing three small-scale features over the slope, identified as "eddy-a," "eddy-b," and "eddy-c?". The velocity vectors indicating cyclonic circulation of eddy-a and eddy-b are derived from 15-m ADCP data from N–S transect 2, occupied over 1917 on 25 January to 0317 on 26 January. The velocities along the E–W transect to the north (along 36.75°N) are from 15-m ADCP data collected over 1912–2237 on 26 January.

speed of transect 5 (which extends over roughly the same latitude band as transect 1).

[16] The velocity vectors along the N–S slope transects further reveal that the dramatic increase in kinetic energy observed in the upper slope region between 21 and 25 January cannot be attributed to an intensification of the regional mean southward flow. Rather, the increase appears to be due to the appearance of strong currents that vary over relatively short along-slope scales and have strong across-slope components. For the lengthiest transects (transects 3, 5, and 6), the RMS of the cross-slope (east) velocity significantly exceeds the RMS of the along-slope (north) velocity (Table 1).

[17] Small-scale features in the surface thermal field encompassing the slope transects are revealed by the SST images of 25–26 January (Figure 3), the only clear-sky images of our study region during the cruise period. They show a series of small-scale features in the SST field over the slope region between 35.75°N and 36.5°N. The most northern of these features is evidenced by a band of relatively warm water partially encompassing a colder water core. Superimposing the velocities of transect 2 (acquired over 1917 on 25 January to 0317 on 26 January) over the SST image of 0245 on 26 January (Figure 3) indicates that this warm-water band is associated with a cyclonic circulation cell, hereafter eddy-a. To the south of this cell, the ADCP velocities indicate another cyclonic circulation cell (eddy-b in Figure 3) that is coincident with a nearly circular warm water cell in the SST field. To the south of this is another warm water cell that is not well sampled by the ADCP transect, but that may be the signature of a third eddy (labeled "eddy-c?" in Figure 3).

[18] A reasonable conclusion is that the strong small-scale velocities captured by the N–S slope transects of 25–30 January are largely due to a series of eddies, which appeared in the slope region between the surveys of 21 and 25 January.

5. Properties of the Eddy Field

[19] Contours of the eastward/westward velocity component over the seven slope transects of 25–30 January (Figure 4) show that the strong kinetic energy of these transects is due to velocities that vary over a wide range of horizontal and vertical length scales. The largest-scale velocity features are bands of eastward and westward flows that extend over most or all of the transect depth (to 267 m) and over horizontal distances of 10–30 km. Accompanying these are much

Table 1. Statistical Properties of the Velocities Measured Over Each North-South Slope Transect of the Winter FINCH Cruise[a]

Transect	Times	⟨Longitude⟩ °W	Latitude °N	u_{RMS} (cm s^{-1})	v_{RMS} (cm s^{-1})	$\langle u^2 + v^2 \rangle$ (cm^2 s^{-2})
1	1113–1823, 21 Jan	74.67	35.75–36.50	11.5	15.0	356
2	1917, 25 Jan to 0317, 26 Jan	74.66	36.01–36.50	17.5	27.5	1063
3	2357, 26 Jan to 0642, 27 Jan	74.66	35.75–36.71	18.0	21.2	774
4	1402–1957, 28 Jan	74.50	36.01–36.50	21.9	19.3	851
5	2252, 28 Jan to 0542, 29 Jan	74.66	35.75–36.49	18.4	30.4	1264
6	1307–2012, 29 Jan	74.66	36.02–36.65	18.2	29.6	1210
7	0532–0802, 30 Jan	74.67	36.25–36.50	15.6	15.4	480
8	1642–1917, 30 Jan	74.67	35.75–36.00	27.0	22.9	1252

[a]The root mean square of the east and north velocity component (u_{RMS} and v_{RMS}, respectively) and the mean of the squared current speed ($\langle u^2 + v^2 \rangle$) were computed from velocities acquired by the shipboard acoustic Doppler current profiler in the 15–267-m depth band.

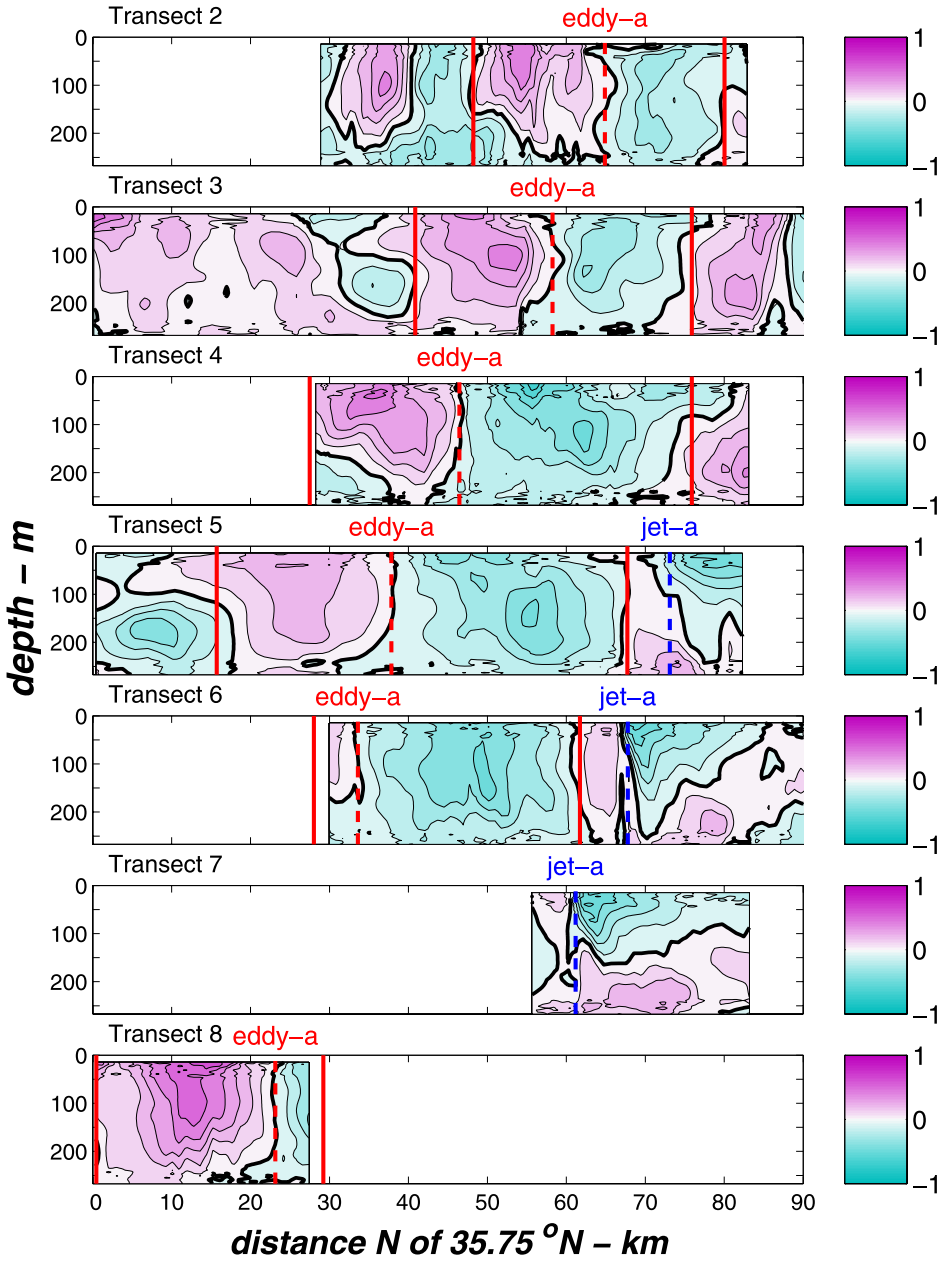

Figure 4. Contours eastward/westward (positive eastward) velocity (m s^{-1}) along the seven N–S slope sections of late January that display the signals of intense eddies. The solid vertical red lines enclose the velocities of eddy-a, and the dashed red lines mark the estimated locations of the eddy's velocity reversal. The dashed blue lines mark the maximum near-surface horizontal velocity gradient of jet-a.

smaller-scale flows that are confined to vertical bands of order 100 m and horizontal distances of order 10 km. These smaller-scale flows appear near the surface in some transects, as exemplified by the shallow eastward currents seen between 0 and 15 km north of 35.75°N in transect 3 (Figure 4). They also are seen at depth. A notable example is the strong eastward flow seen at >100 m and between 0 and 18 km north of 35.75°N in transect 5.

[20] The temperature and salinity fields of the 25–30 January slope transects (Figures 5 and 6) span a broad range of values, 9.2–19.3°C and 33.6–36.3 psu. A feature seen in the three fields determined from the shipboard CTD data (transects 3–5) is a layer of relatively warm (13–14.5°C) and saline (35–35.6 psu) water bracketed above and below by colder and less saline fluid. Other features of note are bands of warm and saline water appearing near the surface in transects 3, 4, 6, and 7, and thin filaments of relatively cold and fresh water appearing at depth in transects 5, 6, and 8. The likely origins of these water masses are considered in section 6.1.

[21] Although the velocity fields of the 25–30 January transects are complex, well-defined features can be identified and traced through a number of transects. One such feature is the cyclonic circulation cell identified as eddy-a above (Figure 3). In the contoured eastward/westward velocity fields of transects 2–6 and 8 (Figure 4), this appears as

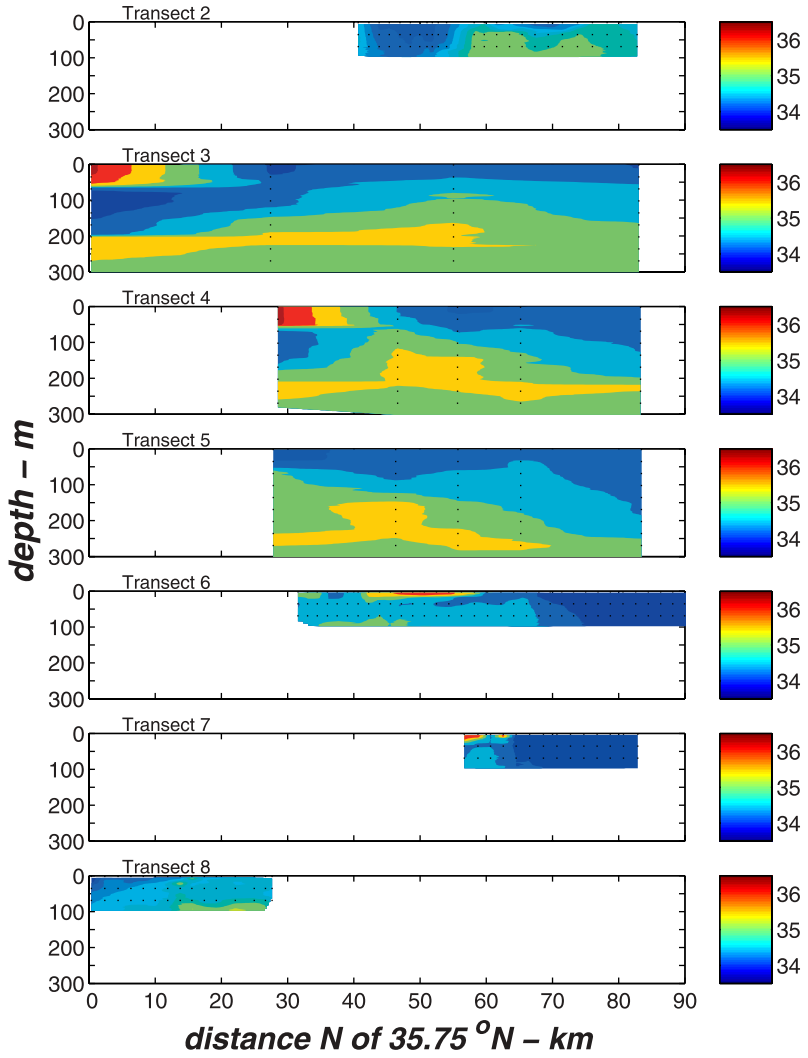

Figure 5. The salinity fields of the seven N–S slope transects of late January. The fields of transects 2, 6, 7, and 8 (3–5) are derived from scanfish (shipboard) CTD measurements. Vertical lines indicate profile locations.

adjacent bands of westward and eastward velocity, with the westward velocity band further north. Another prominent flow feature is a cell of strong westward velocities, which exceed 40 cm s^{-1}, appearing in the northern portion of transects 5–7. As this westward flow is not matched by an adjacent band of eastward flow, it does not appear to be part of an eddy and is referred to as jet-a.

[22] In the contoured velocity fields, the signatures of eddy-a and jet-a shift to the south over time. The rate of eddy-a's movement to the south may be estimated by tracking its velocity reversal as seen in eastward/westward velocity fields of the transects. Plotting the position of this velocity reversal against time (Figure 7) reveals a steady southward translation rate of roughly 10 cm s^{-1}. The estimated southward translation rate of jet-a, determined by tracking location of its maximum horizontal velocity gradient, is also near 10 cm s^{-1} (Figure 7).

[23] It is worthwhile noting that mean southward velocity measured in the 17–265-m depth band over transect 1 is 9.4 cm s^{-1}, roughly equivalent to the southward translation rate of eddy-a and jet-a. Because this transect's velocity field (not shown) displays no indication of strong eddy motion, its mean velocity may be taken as a rough estimate of the large-scale mean flow over the upper slope. A reasonable conclusion is that the southward movement of strong eddy field observed over the slope during 25–30 January is the result of advection by the large-scale flow field.

6. Case Study: Eddy-a

[24] As noted above, eddy-a appears in six of the slope transects. The data from these transects offer a basis for examining the water properties, mixing environment and dynamics of the eddy.

6.1. Water Properties

[25] To determine if the water comprising eddy-a is predominately from the north, we have compared the potential temperature/salinity (θ/S) properties of the eight CTD stations that intercept the eddy, with the θ/S properties of the

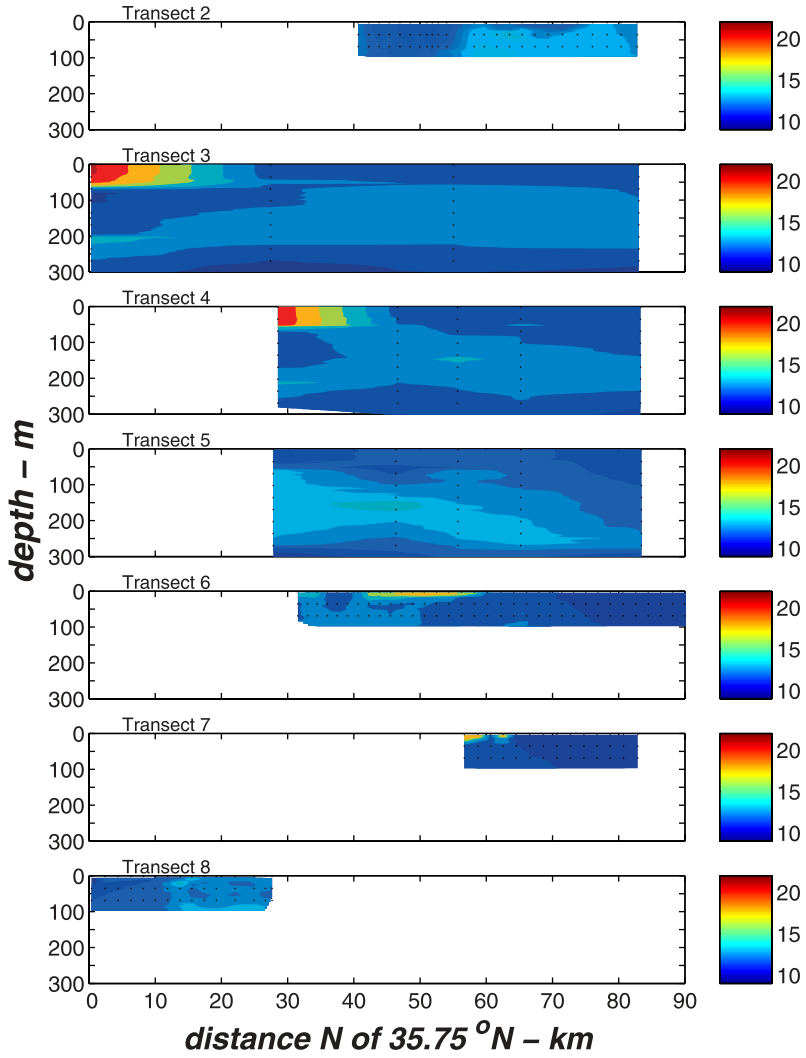

Figure 6. Same as Figure 5, except showing the temperature fields (°C).

CTD transect taken along 36.75°N, at the northern extreme of our study area (Figure 3). Occupied on 26 January, this northern transect extends from the outer shelf (50-m isobath) to the midslope (1500-m isobath). In the SST images of 25–26 January, this transect is situated north of the surface thermal signature of the eddy field intercepted by the N–S slope transects (Figure 3). The water sampled by this transect may thus be regarded as representative of water occupying the southern MAB, north of the eddy field.

[26] This water includes MAB slope water (S > 35), shelf water (S < 34), and water of the MAB shelfbreak front (S > 34 and <35) (Figure 8a). The θ/S properties of these water masses (Figure 8a) form a "Figure 7" pattern typical of the winter-time θ/S property distribution of MAB shelf and slope water [*Beardsley and Flagg*, 1976; *Wright and Parker*, 1976; *Lyne and Csanady*, 1984; *Churchill and Cornillon*, 1991]. The close match between these θ/S properties and the θ/S properties of the water sampled by shipboard CTD stations encompassing eddy-a (Figure 8b) indicate that the eddy was principally a mix of MAB shelf, slope, and shelfbreak frontal water entering the study region from the north. The θ/S comparison further reveals that the eddy contained water originating over a broad isobath range, as the θ/S properties of eddy water closely match the θ/S properties measured at midslope and outer shelf stations along the 36.75°N transect.

[27] The only significant deviation between the θ/S properties measured along the 36.75°N transect and those measured at the shipboard CTD stations within the eddy occurs at the apex of the "Figure 7" with the θ/S properties measured within the eddy extending to higher θ and S. This is due to a band of relatively high θ and S water found over depths 140–180 m at two CTD stations within the eddy (see Figure 9b).

[28] The Scanfish CTD data (Figure 8c) reveal a fourth water mass within the eddy, which is clearly distinct from the water found along the 36.75°N transect. The θ/S properties of this fourth water mass fall along a line of increasing θ and S that terminates at a θ/S combination (19.4°C and 36.3) characteristic of near-surface Gulf Stream water [*Churchill and Cornillon*, 1991]. This intrusion of near-surface Gulf Stream water is shallow but of significant horizontal extent. It appears in the upper 30 m of transect 6 and extends over a distance of 16 km (Figure 5).

[29] To quantify the water mass content of the eddy, we sorted the CTD data acquired within the eddy into catego-

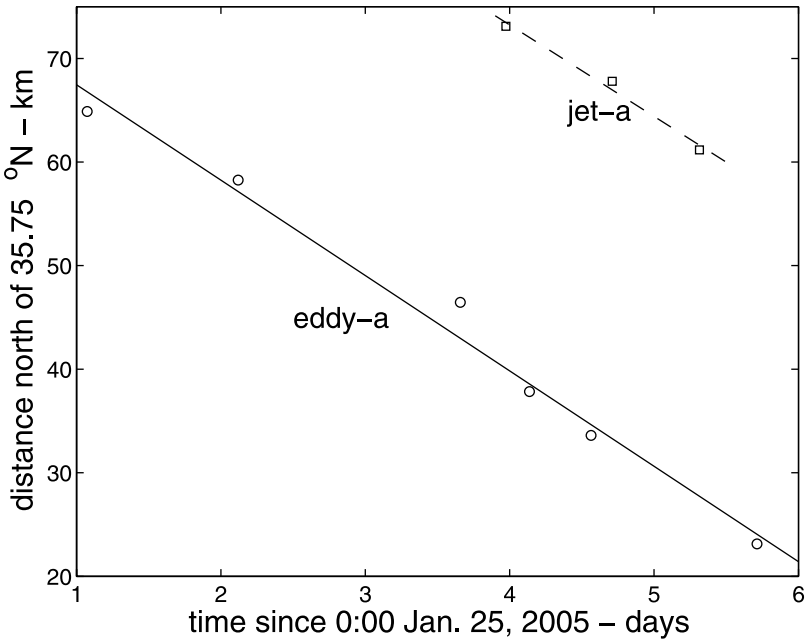

Figure 7. The estimated southward translation rates of eddy-a and jet-a. The open circles show the estimated times and positions of the eastward velocity reversal of eddy-a as seen in the contoured velocity fields of Figure 4. The linear fit to these values (solid line), determined from least squares, has a slope (e.g., estimated eddy translation rate) of -10.5 cm s^{-1}. The open squares show the estimated times and positions of the maximum eastward velocity gradient of jet-a. Their linear fit (dashed line) has a slope of -10.2 cm s^{-1}.

ries of shelf, slope, Gulf Stream, and shelfbreak frontal water based on θ/S criteria (listed in Table 2). For this classification, the Scanfish and shipboard CTD data offer differing views of the eddy with relative advantages and disadvantages. The Scanfish data has much better horizontal resolution than the shipboard data but only extends to 100 m, whereas the shipboard CTD data covers most, if not all, of the eddy's depth. Nevertheless, the Scanfish and shipboard CTD data give similar proportions of shelf and shelfbreak frontal water within the surface 100 m of the eddy (Table 2).

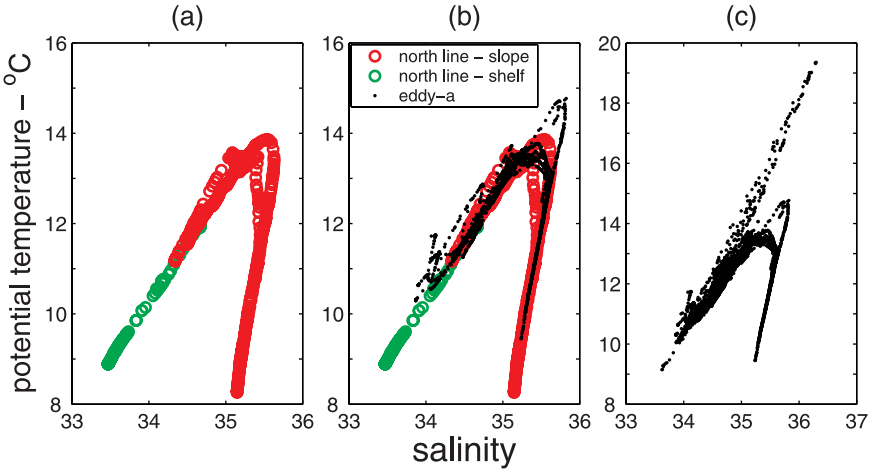

Figure 8. Comparison of the θ/S properties of eddy-a with the θ/S properties of water measured to the north of the eddy field. (a) The θ/S properties measured along a line extending from the midshelf to the upper slope along 36.75°N (Figure 3), with properties from shelf stations (at 51 and 81-m depth) depicted by green circles and properties from shelf edge and slope stations (>160 m) depicted by red circles. (b) The θ/S properties shown in Figure 8a compared with θ/S properties measured at the eight CTD stations that intercepted eddy-a. The close match indicates that much of the water in eddy-a consists of shelf, slope, and shelf edge frontal water from the north. (c) The θ/S properties of all measurements that intercepted eddy-a, from the scanfish and the ship's CTD. These reveal a fourth water mass within the eddy identified as near-surface Gulf Stream water.

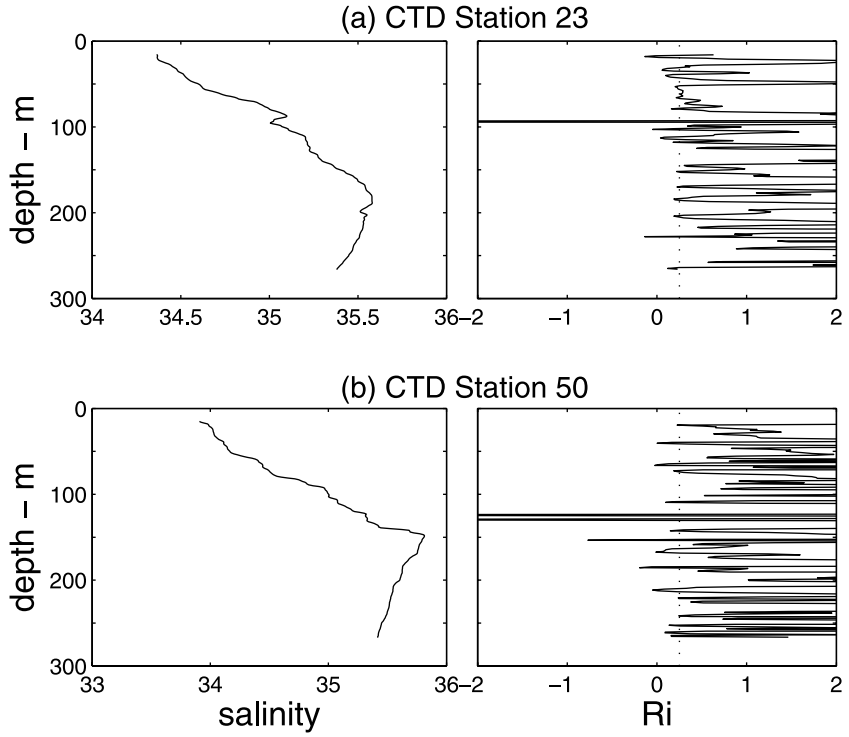

Figure 9. Vertical profiles of salinity and gradient Richardson number at two CTD stations within eddy-a. Stations 23 and 50 are from transects 3 and 4, respectively. The correspondence of low values of Ri, near 0.25, with strong salinity gradients suggests a tendency for water mass mixing within the eddy.

Both data sets indicate that shelfbreak frontal water is the dominant water mass in the upper 100 m of the eddy accounting for roughly 75% of the eddy volume in this depth band. They also reveal that shelf water makes a relatively small contribution, order 5%, to the eddy's volume in the upper 100 m. Over the full eddy, slope water is the dominant water mass, accounting for roughly 64% of its volume.

6.2. Mixing Environment

[30] The various water masses found within the eddy-a overlie one another resulting in considerable vertical stratification of temperature and salinity (Figures 5 and 6). Significantly, strong vertical stratification appears within the upper 50 m. Vertical mixing within the eddy, particularly near the surface, could have significant biological implications. Mixing could, for example, deliver deep nutrients to the euphotic zone or carry phytoplankton out of this zone.

[31] To evaluate the propensity for turbulent vertical mixing within the eddy, we estimated vertical profiles of the gradient Richardson number, *Ri*, according to

$$Ri = \frac{N^2}{C^2} = \frac{\frac{-g}{\rho}\frac{\partial \rho}{\partial z}}{\left(\frac{\partial u_E}{\partial z}\right)^2 + \left(\frac{\partial u_N}{\partial z}\right)^2}$$

where N is the buoyancy frequency, C is the vertical shear, u_E and u_N are east and north velocity components, ρ is potential density, g is gravitational acceleration, and z is depth. N was determined using data from downcasts of the shipboard CTD. For each cast, C was determined from a mean velocity profile computed by averaging all ADCP profiles taken within 30 min and 1 km of the time and location, respectively, of the CTD cast as recorded onboard ship.

Table 2. Percentages of Scanfish and Shipboard CTD Measurements Within Eddy-a That Captured Shelf, Shelf Edge Frontal, Slope, and Near-Surface Gulf Stream Water[a]

		Water Mass Percentages			
Instrument	Depth Range (m)	Shelf	Shelf Edge Front	Slope	Near-Surface Gulf Stream
Scanfish CTD	0–100	3.7	74.1	17.7	4.5
Shipboard CTD	0–100	6.6	81.2	12.2	0
Shipboard CTD	0–300	2.2	34.2	63.6	0

[a]CTD is conductivity-temperature-depth profiler. Shelf ($S <= 34$), shelf edge frontal ($S > 34$ and $S <= 35$), slope ($S > 35$ and $S <= 35.5$ and $\theta <= 14.1$°C; or $S > 35.5$ and $\theta <= 15$°C), and near-surface Gulf Stream ($S > 35$ and $S <= 35.5$ and $\theta > 14.1$°C; or $S > 35.5$ and $\theta > 15$°C) water. The water mass definitions for slope and Gulf Stream water put the warm and saline water at the peak of the "Figure 7" formed by the θ/S properties shown in Figure 8b in the category of slope, and not Gulf Stream, water.

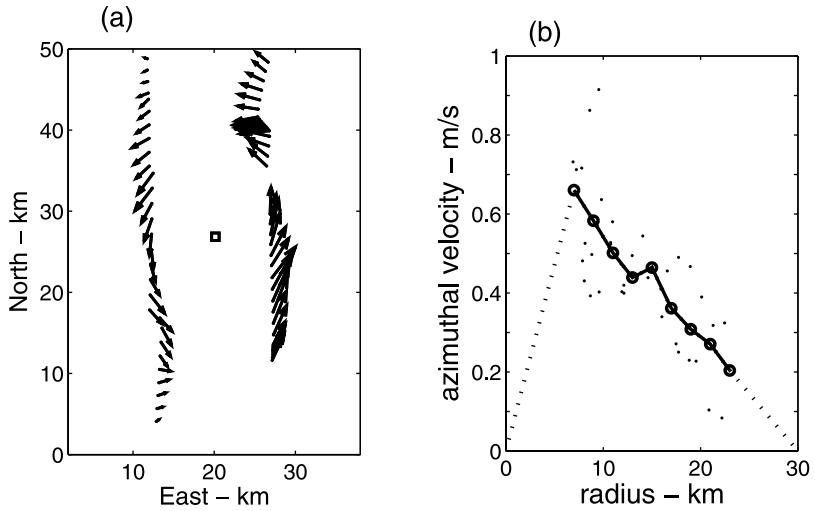

Figure 10. (a) The 15-m velocities from N–S transects 4 and 5 that intercepted eddy-a. The velocities have been translated into an eddy-following coordinate system (see text). The square marks the eddy's center location as determined by minimizing the sum of the squares of the radial velocity component. (b) The azimuthal velocities, computed with the velocities and the center location shown in Figure 10a, are plotted against radius. The solid/dashed line is derived by averaging the estimated azimuthal velocities over 2-km radii bands and extrapolating to zero azimuthal velocity at 0 and 30 km radii.

[32] The resulting *Ri* profiles frequently approach the so-called critical value of 0.25, usually taken as indicative of turbulence generation due to velocity shear (Figure 9). That near critical values of *Ri* often correspond with large vertical salinity gradients reveals a propensity for vertical water mass mixing within the eddy.

6.3. Velocity and Kinetic Energy Distribution

[33] To determine the variation of the eddy's azimuthal velocity (u_θ) with radius, which allows for the estimation of a number of dynamical properties, we employed the velocity data from transects 4 and 5 (Figure 2). These were chosen because they traversed the eddy along different longitude lines and were separated in time by less than 3 h (Table 1). In determining the eddy's u_θ structure using the data from these transects, we first transformed those transect velocities encompassed by the eddy into an eddy following coordinate system. The assumption employed was the eddy translated to the south at a steady rate of $V_T = 10$ cm s^{-1} (Figure 7). To account for this translation, the position of each velocity measurement within the eddy was shifted to the north by a distance of $V_T(t-t_0)$, where t is the time of the velocity measurement and t_0 is the time of the initial velocity measurement taken within the eddy (along transect 4). Because the ADCP measurements presumably include both the velocity field of the eddy and the translation velocity, the latter was subtracted from each ADCP velocity.

[34] The resulting transformed velocities indicate that transects 4 and 5 straddled the eddy's center (Figure 10). To estimate the center location, we derived an expression relating the radial component of each velocity measurement (in the eddy coordinate system) to the center location. At each vertical measurement level, the eddy center location was selected so as to minimize the sum of the squares of the radial velocities, the assumption being that the eddy's flows are principally azimuthal. This procedure was carried out in steps, with the goal of filtering out unusually high radial velocities from the determination of center location. In the first step, the eddy center location was determined using all velocities deemed to be within the eddy's perimeter. Velocities with a radial component that either exceeded 25 cm s^{-1} or was greater than 0.5 of the total velocity magnitude were excluded from the subsequent determination of center location.

[35] The center locations thus computed are all situated between transects 4 and 5 (Figure 10a) and within 6.5 km of one another. The estimates of u_θ determined using the ADCP data and these center locations, extend over a radius band of roughly 5–25 km (Figure 10b). In the surface 150 m, the velocity estimates show a clear tendency to decline with increasing radius. The rate of decline in the surface 50 m has a linear trend (e.g., Figure 10b and Figure 11a) that corresponds to an azimuthal velocity gradient (du_θ/dr) on the order of 3×10^{-5} s^{-1}.

[36] At most levels, the estimated azimuthal velocities do not show a decline with decreasing radius toward the center of the eddy, suggesting that such a decline must occur principally within the innermost 5–7 km radius band not encompassed by the velocity estimates. The implied velocity gradients within this band are large. In the upper 100 m, the estimated azimuthal velocity at 5-km radius is on the order of 0.5 m s^{-1}. Assuming a linear decline of u_θ from this value to zero at the eddy center gives an azimuthal velocity gradient of order 1×10^{-4} s^{-1}, which is comparable with the local value of f (8.6×10^{-5} s^{-1}).

[37] The departure of the eddy's currents from geostrophy may be explored using the equation of motion for an axially symmetric eddy

$$\frac{u_\theta^2}{r} + fu_\theta = \frac{1}{\rho}\frac{\partial P}{\partial r} = fu_{\theta g}$$

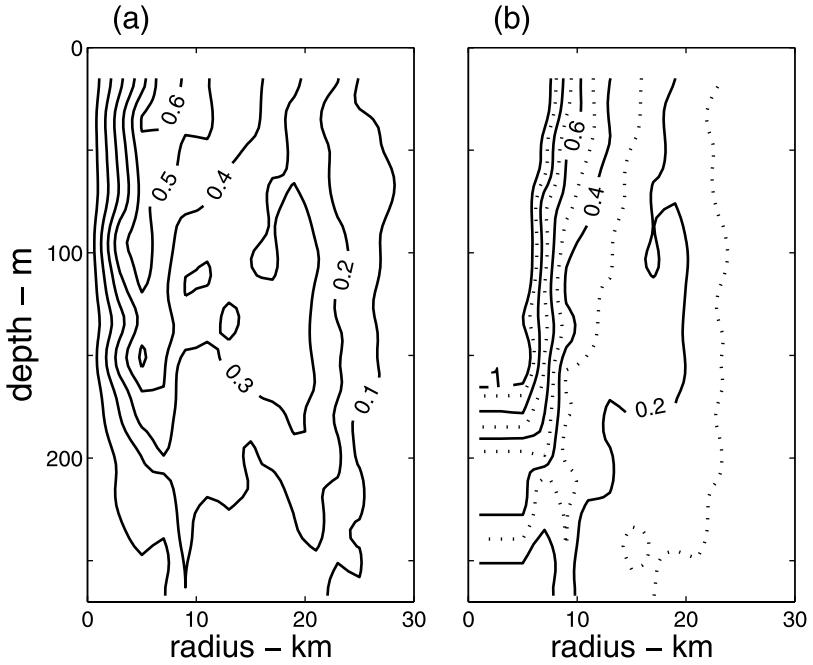

Figure 11. (a) Smoothed distribution of estimated azimuthal velocity (m s^{-1}) of eddy-a as a function of radius and depth. The velocities in the eddy interior (roughly the inner 5 km) have been linear extrapolated from the innermost velocity estimate to zero velocity at zero radius (Figure 10b). (b) Distribution of $\frac{u_\theta}{fr}$ (a measure of ageostrophy) over eddy-a as computed from the u_θ distribution in Figure 11a.

where $u_{\theta g}$ is the geostrophic velocity and P is pressure at a depth stratum. The deviation of the total flow from geostrophy in such an eddy is described by

$$u_{\theta g} = u_\theta \left(1 + \frac{u_\theta}{fr}\right),$$

where the $\frac{u_\theta}{fr}$ term is a measure of the flow's departure from geostrophy. To estimate the distribution of this term, we created a spatial distribution of $u_\theta(r,z)$ from the various individual estimates of azimuthal velocity. In the radius band encompassing the azimuthal velocity estimates, $u_\theta(r,z)$ was set equal to the averages of the velocity estimates in 2-km

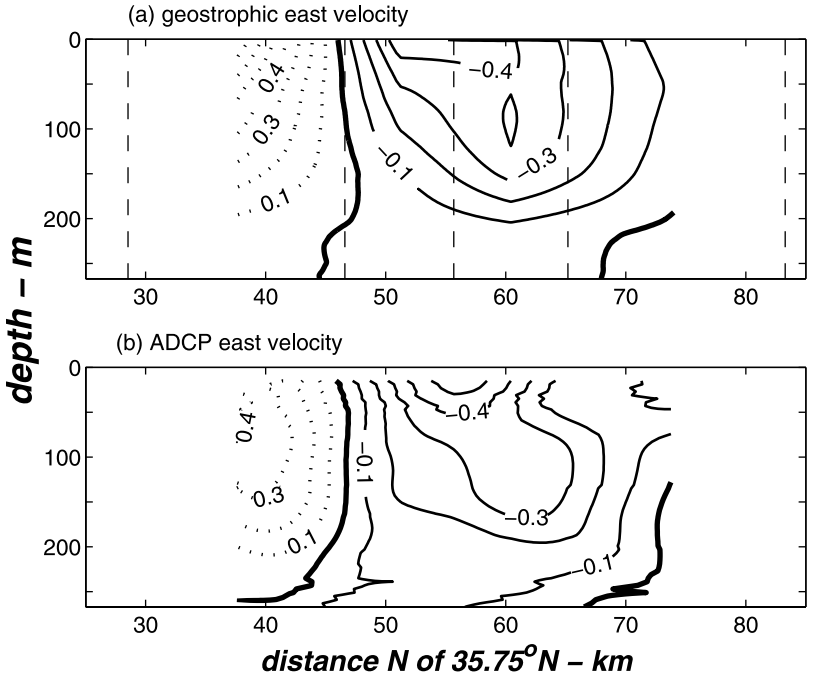

Figure 12. Comparison of (a) eastward geostrophic velocity (m s^{-1}) computed from the CTD data of N–S slope transect 4 with (b) the smoothed ADCP eastward velocity distribution along the same transect. The vertical dashed lines in Figure 12a mark the locations of the CTD stations.

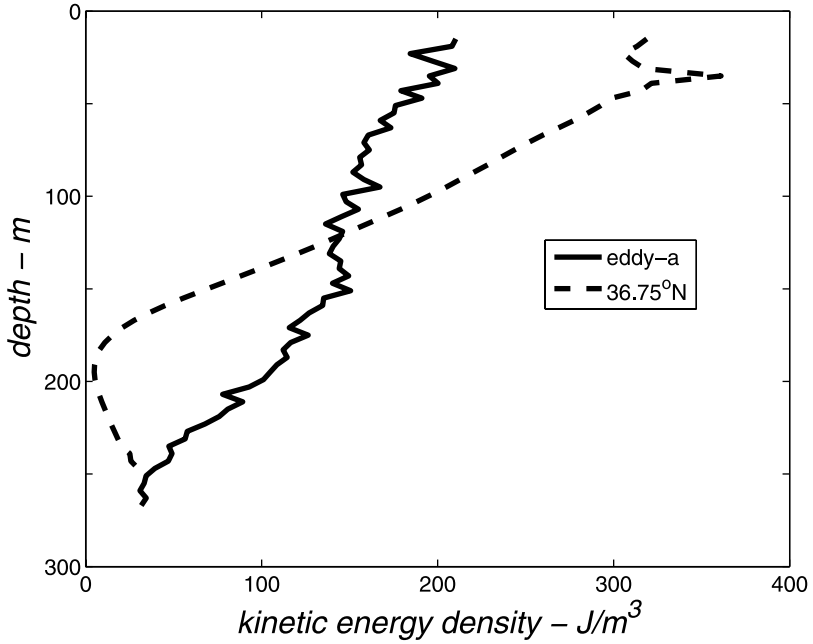

Figure 13. Kinetic energy density of eddy-a (solid line) and the shelf edge frontal jet (dashed line) as a function of depth.

radius segments (Figure 10b). $u_\theta(r,z)$ was linearly extrapolated from the margins of this band to equal zero at the $r = 0$ and $r = R(z)$ (Figure 10b). Because the eddy's size, as judged from the distribution of the azimuthal velocity estimates, appears to decline with depth, the outermost eddy radius, $R(z)$, was set equal to 30 km for z < 175 m and to 26 km for z > = 175 m.

[38] Estimates of $\frac{u_\theta}{fr}$, derived from a smoothed form of u_θ, indicate a significant departure from geostrophy near the center of the eddy. These estimates are of order 1 and larger over an area reaching to a depth of 180 m and extending from the eddy's center to radii of between 5 and 7.5 km (Figure 11b). Nevertheless, near geostrophic conditions appear to prevail over much of the eddy, as the estimates $\frac{u_\theta}{fr}$ are less than 0.3 over 67% of the eddy.

[39] Importantly, near geostrophic conditions are indicated over much of those portions of transects 4 and 5 that intercept the eddy. In particular, estimates of $\frac{u_\theta}{fr}$ are small (<0.3) over transect segments that sample the large eastward velocities of the eddy, which typically occurs at $r > 10$ km (see Figure 10a). Geostrophic velocities computed using the CTD data from these transects thus offer a reasonable representation of the baroclinic velocity field of the eddy.

[40] For both transects, the eastward geostrophic velocities calculated with the CTD data and referenced 280 m (the deepest common depth of the CTD profiles) show a similar structure to the smoothed eastward velocity distribution derived from the ADCP data (Figure 12). Significantly, the geostrophic velocities show large vertical shears distributed over the upper 250 m that are nearly matched by the vertical shears of the ADCP velocities. Clearly, the baroclinic velocities of eddy-a extend to a depth of order 250 m.

[41] The kinetic energy density (KED, energy per unit volume) and total kinetic energy (KE) of the eddy may be estimated according to

$$KED(z) = \frac{\rho \int_0^{R(z)} u_\theta^2(r,z) r dr}{R^2(z)}$$

$$KE = \int_{-H}^{0} \left| \pi R^2(z) KED(z) dz \right|$$

where ρ is the density of seawater (taken as 1024 kg m^{-3}) and H is the total depth of the eddy. As would be inferred from the distribution of baroclinic velocities within the eddy, the kinetic energy density exhibits a modest decline with depth in the upper 200 m (Figure 13). The estimated total kinetic energy is 2.4×10^{13} J. For comparison, *Olson et al.* [1985] estimated the total kinetic energy of a Gulf Stream warm-core ring (ring 82B) to be nearly two order of magnitude higher, at 1×10^{15} J.

[42] The southward translation of eddy-a and the close match of its water properties with shelf/slope water to the north (Figure 8) make the shelfbreak frontal jet a strong candidate as the energy source of the eddy-a and the larger eddy field in which it is embedded. The only measurements of the shelfbreak frontal jet acquired during the observation of eddy-a are from the 26 January transect along 36.75°N (Figure 3). This captures roughly half of the jet, which is evidenced by southward velocities that steadily increase offshore to a value of 0.6 m s^{-1} at the eastern end of the transect (Figure 14). The jet is more than 5 km offshore of the shelfbreak, considerably seaward of the mean frontal jet

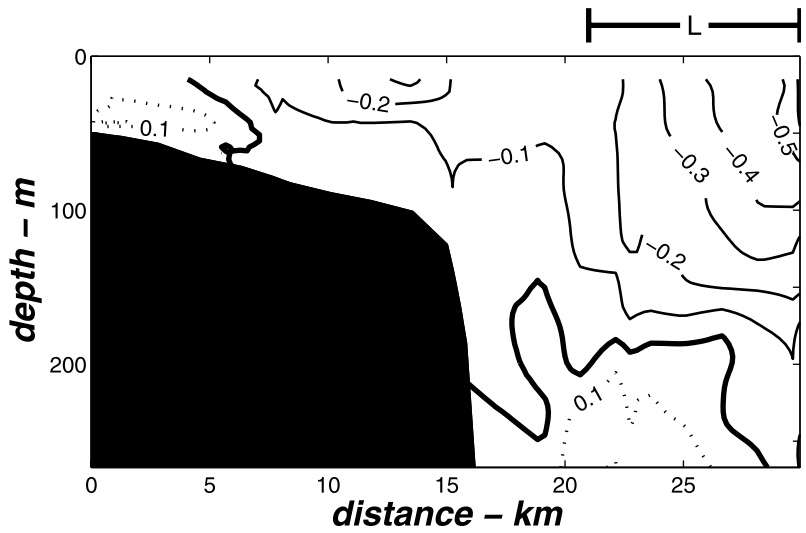

Figure 14. Detided northward velocities (m s^{-1}; positive to the north) measured along the 36.75°N transect (Figure 3). A portion of the shelf edge frontal jet is seen at the eastern end of the transect. The distance range labeled L denotes the band over which the kinetic energy density of the jet was determined.

positions reported by *Linder and Gawarkiewicz* [1998] and *Fratantoni et al.* [2001]. The maximum current of the jet seen in the 36.75°N transect is also considerably greater than the order 0.3 m s^{-1} maximum current of the mean jet flow computed by *Fratantoni et al.* [2001] using 2 years of shipboard ADCP data acquired near 70°W.

[43] Situated beneath the jet is a northward countercurrent with a magnitude of order 10 cm s^{-1} (Figure 14). As revealed by its θ/S characteristics (Figure 8), this countercurrent is comprised of MAB slope water, roughly spanning a θ range of 8.5–12.5°C and a S range of 35.15–35.45. It is interesting to note that the presence of a weak countercurrent beneath the shelfbreak frontal jet appears in the numerical model simulations of *Chapman and Lentz* [1994], done as part of their study of the manner in which the front becomes "trapped" at an isobath on a uniformly sloping shelf.

[44] The kinetic energy density of the portion of the shelfbreak frontal jet intercepted by the 36.75 °N transect may be calculated as

$$KED(z) = \frac{\rho \int_0^L \left[u_E^2(y,z) + u_N^2(y,z)\right] dy}{2L}$$

where y is distance along the jet and L is the integration path over the jet (shown in Figure 14). This energy density is of similar magnitude to the kinetic energy density of eddy-a but decays more rapidly with increasing depth (Figure 13).

[45] Clearly, kinetic energy density cannot be viewed as a conservative quantity. Generation of an eddy through instability of the frontal jet will likely involve conversion of available potential energy to kinetic energy [*Pedlosky*, 1979] and redistribution of the kinetic energy (e.g., through vortex stretching). Nevertheless, one may expect the product of jet instability to have a kinetic energy magnitude similar to that of the parent jet. The similar KED magnitudes of the shelfbreak frontal jet and eddy-a lend support to the notion that eddy-a was generated through instability of the jet. This possibility is considered further in section 7.

6.4. Water Mass Transports

[46] Our assessments of eddy radius and southward translation rate allow for a rough estimation of the rates at which the eddy transports shelf and shelfbreak frontal water to the south. The maximum eddy radii given above and the assumption of a maximum eddy depth of 300 m gives a total eddy volume of 7.6×10^{11} m^3. On the basis of the analysis presented in section 6.1, and summarized in Table 2, we may assume that the eddy contains 2% shelf water and 33% water from the shelfbreak front, putting the volumes of shelf and shelfbreak frontal water within the eddy at 1.5×10^{10} and 2.5×10^{11} m^3, respectively. These volumes would be carried past a given latitude in 6×10^5 s, assuming an eddy southward translation velocity of 0.1 m s^{-1} and eddy diameter of 60 km. The estimated mean rate of southward transport is then 0.025 Sv for shelf water and 0.4 Sv for water from the shelfbreak front. The estimated shelf water transport is relatively small compared with estimates of volume transport over the MAB shelf, which vary from 0.17 to 0.26 Sv [*Beardsley et al.*, 1976; *Biscaye et al.*, 1994; *Churchill and Berger*, 1998; *Kim et al.*, 2001]. However, our estimate of the mean transport of shelfbreak frontal water within the eddy is comparable with published estimates of the transport within the shelfbreak frontal jet. Using data from seven ADCP sections acquired south of Cape Cod, *Fratantoni et al.* [2001] computed a mean transport of 0.46 Sv within the shelfbreak frontal jet, whereas *Rasmussen et al.* [2005] determined shelfbreak jet transports in the range of 0.7–1.3 Sv over four ADCP sections in the southern MAB.

7. Discussion and Summary

[47] Although its total kinetic energy is small compared with that of a Gulf Stream warm-core ring, the dimensions and velocities of eddy-a are nonetheless impressive. Our

analysis indicates that the eddy's baroclinic velocity signature attained a maximum value of roughly 0.7 m s^{-1}, extended over a diameter of order 60 km, and reached a depth of order 250 m. The substantial size and strength of the eddy raise the issue of whether the eddy is characteristic of shelfbreak eddies or an anomaly happened upon by our repeated slope sections. While available data are not sufficient to assemble a climatology of shelfbreak eddies, some insight as to where eddy-a fits in the spectrum of shelfbreak eddies may be gained from a comparison of the eddy's characteristics with those of MAB shelfbreak eddies described in previous published studies.

[48] The velocity structure of shelfbreak eddies over the MAB have been examined, with varying degrees of resolution, by *Houghton et al.* [1986], *Flagg et al.* [1998], and *Gawarkiewicz et al.* [2001]. The anticyclonic eddy observed by *Gawarkiewicz et al.* [2001], south of New England, was relatively small and weak in comparison with eddy-a. Its diameter and maximum azimuthal velocity were of order 30 km and 0.25 m s^{-1}, respectively. The eddy examined by *Flagg et al.* [1998], which appeared over the southern MAB slope, was also anticyclonic and exhibited peak azimuthal velocities of order 0.25 m s^{-1}. Similar to eddy-a, however, this eddy's velocity signature extended to at least 250-m depth (the velocity data examined by Gawarkiewicz et al. were limited to the upper 140 m). The eddy analyzed by *Houghton et al.* [1986] was most similar to eddy-a in size and current strength. Its anticyclonic velocity signature peaked near 0.5 m s^{-1}, and it extended over a diameter of order 50 km and to a depth of at least 200 m.

[49] These prior observations combined with our measurements showing a rich eddy field over the southern MAB slope suggest that shelfbreak eddies span broad ranges of size and current strength. While eddy-a may occupy the top categories of these ranges, its similarity in size and current strength to the eddy observed by *Houghton et al.* [1986] suggest that it is not an anomaly.

[50] The mechanisms by which shelfbreak eddies form in the southern MAB are important from a regional perspective as they provide a means by which outer shelf water and shelfbreak frontal water may be transported to the slope region. The close similarity of θ/S properties and KED magnitudes found within eddy-a and within shelfbreak frontal jet make instability of the frontal jet a likely mechanism by which the eddy was generated. Judging from the velocity distribution measured along 36.75°N (Figure 14), it appears that the jet was a considerable distance seaward of the shelfbreak during the time of our cruise. Eddy generation via instability of the frontal jet at such a location would not be vertically constrained by the bottom depth. The order 300-m depth and considerable slope water volume in eddy-a (Figure 4 and Table 2) are thus not inconsistent with the notion that the eddy was generated by instability of the front.

[51] The stability of the MAB shelfbreak frontal jet has recently been explored by *Lozier et al.* [2002]. Employing a linear stability analysis in three dimensions, they found the jet to be unstable over a wide range of configurations as determined by varying jet width, depth, and maximum current speed. For a jet configuration approximating that seen to the north of our study region (Figure 14), with a width of 20 km and a maximum velocity of 0.6 m s^{-1}, their analysis indicated growth rates of order 1 d^{-1} for perturbations of 10–50 km. This is consistent with the appearance of the order 60 km diameter eddy-a in the 4 days between the first and second transects of our slope surveys.

[52] Given the propensity of jet instability indicated by the analysis of *Lozier et al.* [2002], it seems likely that shelfbreak eddy formation may be a common occurrence in the southern MAB. Our observations suggest that such eddy formation may entrain a substantial quantity of water and kinetic energy from the shelfbreak jet and the outer shelf region. The broad range of θ/S properties and favorable conditions for vigorous turbulent mixing found in eddy-a indicate that shelfbreak eddies may be important agents in mixing the disparate water masses found in the southern MAB. Such mixing likely has significant ecological consequences, as in bringing temperate and warm water species in close contact, that have yet to be fully explored.

[53] **Acknowledgments.** We are grateful to Captain L. Bearse and crew of the R/V *Oceanus* for expert support of the scientific operations during the trying conditions of the FINCH 2005 winter cruise. Our thanks go to B. Kidd, C. Marquette, and W. Ostrom for their work in acquiring the data during the cruise. Particular thanks go to F. Bahr and C. Linder who participated in the cruise operations and contributed significantly to the analysis of the data presented here. This work was supported by the U.S. National Science Foundation through grant OCE-03-27249.

References

Beardsley, R. C., and W. C. Boicourt (1981), On estuarine and continental shelf circulation in the Middle Atlantic Bight, edited by B. A. Warren and C. Wunsch, in *Evolution of Physical Oceanography*, pp. 198–233, MIT Press, Cambridge, Mass.

Beardsley, R. C., and C. N. Flagg (1976), The water structure, mean currents and the shelf-water/slope-water front on the New England continental shelf, *Mem. Coc. R. Sci. Liege*, *10*, 209–225.

Beardsley, R. C., W. C. Boicourt, and D. V. Hansen (1976), Physical oceanography of the Middle Atlantic Bight, edited by M. G. Gross, in *Middle Atlantic Continental Shelf and the New York Bight, Spec. Symp.*, vol. 2, pp. 20–34, Am. Soc. of Limnol. and Oceanogr., Gloucester Point, Va.

Bigelow, H. B. (1933), Studies of the waters on the continental shelf, Cape Cod to Chesapeake Bay, I. The cycle of temperature, *Pap. Phys. Oceanogr. Meteorol.*, *2*(4), 1–136.

Biscaye, P. E., C. N. Flagg, and P. E. Falkowski (1994), The Shelf Edge Exchange Processes experiment. SEEP-II: An introduction to hypotheses, results, and conclusions, *Deep Sea Res., Part II*, *41*, 231–252, doi:10.1016/0967-0645(94)90022-1.

Blanton, B. O., R. A. Luettich, F. Werner, and H. Seim (2004), Barotropic tides in the South Atlantic Bight, *J. Geophys. Res.*, *109*, C12024, doi:10.1029/2004JC002455.

Chapman, D. C. (1986), A simple model of the formation and maintenance of the shelf/slope front in the Middle Atlantic Bight, *J. Phys. Oceanogr.*, *16*, 1273–1279, doi:10.1175/1520-0485(1986)016<1273:ASMOTF> 2.0.CO;2.

Chapman, D. C., and S. J. Lentz (1994), Trapping of a coastal density front by the bottom boundary layer, *J. Phys. Oceanogr.*, *24*, 1464–1478, doi:10.1175/1520-0485(1994)024<1464:TOACDF>2.0.CO;2.

Churchill, J. H., and T. J. Berger (1998), Transport of Middle Atlantic Bight shelf water to the Gulf Stream, *J. Geophys. Res.*, *103*, 30605–30621, doi:10.1029/98JC01628.

Churchill, J. H., and P. C. Cornillon (1991), Water discharged from the Gulf Stream north of Cape Hatteras, *J. Geophys. Res.*, *96*, 22,227–22,243, doi:10.1029/91JC01877.

Churchill, J. H., P. C. Cornillon, and P. H. Hamilton (1989), Velocity and hydrographic structure of subsurface shelf water at the Gulf Streams edge, *J. Geophys. Res.*, *94*, 10791–10800, doi:10.1029/JC094iC08p10791.

Churchill, J. H., J. P. Manning, and R. C. Beardsley (2003), Slope water intrusions onto Georges Bank, *J. Geophys. Res.*, *108*(C11), 8012, doi:10.1029/2002JC001400.

Fairbanks, R. G. (1982), The origin of continental shelf and slope water in the New York Bight and Gulf of Maine: Evidence from $H_2^{18}O/H_2^{16}O$ ratio measurements, *J. Geophys. Res.*, *87*, 5796–5808, doi:10.1029/JC087iC08p05796.

Flagg, C. N., D. Wallace, and Z. Kolber (1998), Cold anticyclonic eddies formed from cold pool water in the southern Middle Atlantic Bight, *Cont. Shelf Res.*, *17*, 1839–1867, doi:10.1016/S0278-4343(97)00038-1.

Ford, W. L., J. R. Longard, and R. E. Banks (1952), On the nature, occurrence and origin of cold, low salinity water along the edge of the Gulf Stream, *J. Mar. Res.*, *11*, 281–293.

Fratantoni, P. S., R. S. Pickart, D. J. Torres, and A. Scotti (2001), Mean structure and dynamics of the shelfbreak jet in the Middle Atlantic Bight during fall and winter, *J. Phys. Oceanogr.*, *31*, 2135–2156, doi:10.1175/1520-0485(2001)031<2135:MSADOT>2.0.CO;2.

Garvine, R. W., K.-C. Wong, G. Gawarkiewicz, R. K. McCarthy, R. W. Houghton, and F. Aikman III (1988), The morphology of shelf break eddies, *J. Geophys. Res.*, *93*, 15,593–15,607, doi:10.1029/JC093iC12p15593.

Gawarkiewicz, G., F. Bahr, R. C. Beardsley, and K. H. Brink (2001), Interaction of a slope eddy with the shelfbreak front in the Middle Atlantic Bight, *J. Phys. Oceanogr.*, *31*, 2783–2796, doi:10.1175/1520-0485(2001)031<2783:IOASEW>2.0.CO;2.

Halkin, D., and T. Rossby (1985), The structure and transport of the Gulf Stream at 73°W, *J. Phys. Oceanogr.*, *15*, 1439–1452, doi:10.1175/1520-0485(1985)015<1439:TSATOT>2.0.CO;2.

Halliwell, G. R., Jr., and C. N. K. Mooers (1983), Meanders of the Gulf Stream downstream of Cape Hatteras 1975–1978, *J. Phys. Oceanogr.*, *13*, 1275–1292, doi:10.1175/1520-0485(1983)013<1275:MOTGSD>2.0.CO;2.

Houghton, R. W., D. B. Olson, and P. J. Celone (1986), Observation of an anticyclonic eddy near the continental shelf break south of New England, *J. Phys. Oceanogr.*, *16*, 60–71, doi:10.1175/1520-0485(1986)016<0060:OOAAEN>2.0.CO;2.

Kim, Y. Y., G. L. Weatherly, and L. J. Pietrafesa (2001), On the mass and salt budgets for a region of the continental shelf in the southern Mid-Atlantic Bight, *J. Geophys. Res.*, *106*, 31263–31282, doi:10.1029/2000JC000738.

Libby, W. (1891), Report upon the physical investigation of the waters off the southern coast of New England, made during the summer of 1889 by the U.S. Fisheries schooner *Grampus*, *U.S. Fish Wildl. Serv. Fish. Bull.*, *9*, 391–459.

Lillibridge, J. L., III, G. Hitchcock, T. Rossby, E. Lessard, M. Mork, and L. Golmen (1990), Entrainment and mixing of shelf/slope waters in the near-surface Gulf Stream, *J. Geophys. Res.*, *95*, 13,065–13,087, doi:10.1029/JC095iC08p13065.

Linder, C. A., and G. Gawarkiewicz (1998), A climatology of the shelfbreak front in the Middle Atlantic Bight, *J. Geophys. Res.*, *103*, 18,405–18,423, doi:10.1029/98JC01438.

Lozier, M. S., M. S. C. Reed, and G. G. Gawarkiewicz (2002), Instability of a shelfbreak front, *J. Phys. Oceanogr.*, *32*, 924–944, doi:10.1175/1520-0485(2002)032<0924:IOASF>2.0.CO;2.

Luettich, R. A., J. J. Westerink, and N. W. Scheffner (1992), ADCIRC: An advanced three-dimensional circulation model for shelves, coasts and estuaries, Report 1: Theory and methodology of ADCIRC-2DDI and ADCIRC-3DL, *Tech. Rep. DRP-92-6*, U.S. Army Eng. Waterw. Exp. Stn., Vicksburg, Miss.

Lyne, V. D., and G. T. Csanady (1984), A compilation and description of hydrographic transects of the Mid-Atlantic Bight shelf-break front, *Tech. Rep. WHOI-84-19*, 290 pp., Woods Hole Oceanogr. Inst., Woods Hole, Mass.

Olson, D. B., R. W. Schmitt, M. Kennelly, and T. M. Joyce (1985), A two-layer diagnostic model of the long-term physical evolution of warm-core ring 82B, *J. Geophys. Res.*, *90*, 8813–8822.

Pedlosky, J. (1979), *Geophysical Fluid Dynamics*, 624 pp., Springer, New York.

Pickart, R. S., and D. R. Watts (1993), Gulf Stream meanders over steep topography, *J. Geophys. Res.*, *98*, 6895–6905, doi:10.1029/92JC02792.

Rasmussen, L., G. Gawarkiewicz, W. B. Owens, and M. S. Lozier (2005), Slope water, Gulf Stream, and seasonal influences on southern Mid-Atlantic Bight circulation during the fall-winter transition, *J. Geophys. Res.*, *110*, C02009, doi:10.1029/2004JC002311.

Wright, W. R., and C. E. Parker (1976), A volumetric temperature/salinity census for the Middle Atlantic Bight, *Limnol. Oceanogr.*, *21*, 563–571.

J. H. Churchill and G. Gawarkiewicz, Department of Physical Oceanography, Woods Hole Oceanographic Institution, Woods Hole, MA 02543, USA. (jchurchill@whoi.edu)